scientific reports

Check for updates

OPEN

Lapatinib ameliorates skin fibrosis by inhibiting TGF-β1/Smad and non-Smad signaling pathway

Yongping Wang[1,3], Tiantian Zhang[2,3], Hao Song[1]✉ & Cheng Yang[2]✉

Skin fibrosis, characterized by excessive accumulation of extracellular matrix (ECM) in the dermis, can lead to hypertrophic scars and impaired mobility. The ErbB family of receptor tyrosine kinases, including ErbB1 and ErbB2, plays a crucial role in organ fibrosis, but their specific impact on skin fibrosis is less understood. This study investigated the role of ErbB1 and ErbB2 in skin fibrosis and the therapeutic potential of lapatinib, a dual ErbB1 and ErbB2 tyrosine kinase inhibitor. Using qPCR, cell culture assays, Western blotting, and in vivo models, we found significant upregulation of ErbB1 and ErbB2 in keloid tissues and fibroblasts. Lapatinib treatment resulted in a dose-dependent decrease in ErbB1 and ErbB2 expression, which suppressed the expression of fibroblast activation markers. Our findings suggest that lapatinib may be a promising therapeutic agent for skin fibrosis by targeting ErbB1/ErbB2 and modulating the TGF-β1/Smad2/3/Erk/Akt signalling pathways. These results warrant further clinical investigation into lapatinib for treating skin fibrosis and related conditions.

Keywords Skin fibrosis, Keloid, Systemic sclerosis, Fibroblasts, Lapatinib, TGF-β1 signaling pathways

Fibrosis is characterized by the pathological accumulation of extracellular matrix (ECM) proteins, predominantly collagen, which supplant functional connective tissue[1]. This process culminates in the emergence of fibrotic scars, an inevitable outcome of the wound healing response after tissue injury[2]. Skin fibrosis may arise as a localized reaction to dermal harm resulting from burns, surgical procedures, mechanical trauma, infections, or irradiation, representative diseases such as keloids. It can also be associated with systemic autoimmune disorders such as systemic sclerosis (SSc). Systemic sclerosis is an idiopathic systemic autoimmune rheumatic disease that the key manifestation is progressive skin fibrosis[3]. Keloids are benign, tumour-like fibrous overgrowths that manifest as an exaggerated healing response to dermal injury[4]. The development of these skin fibrosis diseases is governed by a sophisticated and stringently regulated sequence of events encompassing several overlapping phases: maintaining tissue equilibrium, protracted inflammation, excessive ECM synthesis and deposition, and amplified fibroblast proliferation[5]. The affliction caused by skin fibrosis imposes a considerable burden on affected individuals, encompassing aesthetic disfigurement, sensory discomfort such as pruritus, pain, and, in extreme cases, restrictions in joint mobility.

The transmembrane receptor tyrosine kinases (RTKs) of the ERBB family, comprised of epidermal growth factor receptor EGFR (ErbB1), HER2 (ErbB2), HER3 (ErbB3), and HER4 (ErbB4)[6], play pivotal roles in various physiological and pathological processes. Upon ligand binding to the extracellular domains of ErbB1, ErbB3, and ErbB4, the formation of catalytically active heterooligomeric complexes is initiated[7]. Accumulating evidence has indicated that all ErbB members participate in the pathogenesis of organ fibrosis[8–13]. Although their specific role in skin fibrosis has not been extensively explored, it is hypothesized that the ErbB family may exert significant effects on this condition since organ fibrosis has a common effector cell, fibroblasts. To test whether the ErbB family is involved in skin fibrosis, we conducted a quantitative polymerase chain reaction (qPCR) assay to quantify the expression levels of the ErbB family members in keloid tissues and fibroblasts. Our findings revealed a marked increase in the expression of ErbB1 and ErbB2 compared with that in normal skin samples.

Lapatinib, a dual ErbB1 and ErbB2 tyrosine kinase inhibitor that is already an established treatment for breast cancer[14], reversibly binds to the intracellular ATP binding site of the tyrosine kinase domain and prevents receptor phosphorylation and activation, thereby blocking downstream signalling pathways such as the MAPK/Erk and PI3K/Akt pathways, which are involved in cell survival and proliferation, respectively[15], and some studies have shown that lapatinib serves as a potential treatment for some skin-related diseases, such as

[1]Frontier Science Center for Synthetic Biology (Ministry of Education), Key Laboratory of Systems Bioengineering, School of Chemical Engineering and Technology, Tianjin University, Tianjin 300350, China. [2]State Key Laboratory of Medicinal Chemical Biology, College of Pharmacy, Nankai University, Tianjin, China. [3]Yongping Wang and Tiantian Zhang contributed equally to this paper. ✉email: hsong@tju.edu.cn; cheng.yang@nankai.edu.cn

metastatic squamous cell carcinoma of the skin[16,17]. Encouraged by these findings, we investigated the potential therapeutic efficacy of lapatinib. The effectiveness of lapatinib was evaluated in both in vitro and in vivo models of two types of skin fibrosis, keloid and systemic sclerosis, in this study.

Materials and methods

Human skin fibroblasts separation and culture

Keloid fibroblasts are isolated from keloid tissue from keloid patients, and normal human fibroblast are obtained from residual skin tissue during reconstruction surgery, both kinds of skin tissue are from the Tianjin Academy of Traditional Chinese Medicine Affiliated Hospital. All participants in our research signed an informed consent before study, and all methods were performed in accordance with the Ethics Committee of Nankai University (approval No. NKUIRB2021116). The isolated fibroblasts were cultured with 15% fetal bovine serum (ExCell Bio.) in DMEM (Beijing Solarbio Science & Technology Co., Ltd.).

Mouse primary skin fibroblast separation and culture

Within the laminar flow hood, neonatal mice of less than one day old were sacrificed by cervical dislocation. Initially, the mice were immersed in a 5% povidone-iodine solution for two minutes, followed by an immersion in 70% ethanol. Subsequently, they were rinsed thoroughly with sterile water and placed in a sterile petri dish for further use. The intact dermal layer of the mouse skin was excised and placed in a sterile petri dish, ensuring that the skin was fully spread out. The dish was then refrigerated at 4 °C for a period of 2 h to allow the tissue to set. Freshly prepared cold trypsin solution was gently poured into the petri dish, and then the petri dish was sealed and left to incubate overnight in a 4 °C refrigerator. To each dermis, 2 mL of collagenase solution was added, and the tissue was incubated at 37 °C in a water bath for 30 min. Subsequently, DNase solution was added to each dermis, and the incubation was continued for an additional 10 min. After filtration through a mesh screen, the resulting solution was centrifuged to obtain primary dermal fibroblasts from the mouse skin. These cells were cultured for subsequent experiments.

BLM-induced skin fibrosis murine model

Select male C57BL/6J wild-type mice (age 8–10 weeks, 20–22 g) were bought from Beijing Vital River Laboratory Animal Technology (Beijing, China). The animal experiments were conducted by the Institutional Animal Care and Use Committee (IACUC) of Nankai University (No. SYXK 2019-0001). For model establishment part, mice were anesthetized via intraperitoneal injection of sodium pentobarbital, then gently remove the dorsal hair of approximately 2 × 2 cm using an electric shaver. Induce the formation of skin fibrosis by subcutaneous injection of 100 μL of 0.5U bleomycin into the same skin area for a duration of 3 weeks. A total of 35 mice were evenly distributed across five distinct experimental groups, with each comprising 7 individuals. The grouping is as follows: (1) Control group, was administered a daily intradermal injection of 100 μL of sterile saline solution; (2) Model group, received a daily intradermal injection of 100 μL of BLM solution; (3–5) Treatment groups, receiving daily intradermal injections of a mixture of 100 μL BLM solution with lapatinib (at concentrations of 5, 10, and 20 μM, respectively). After 21 days of continuous injection, euthanize the mice by cervical dislocation, harvest the dorsal skin, and analyze the histopathological changes in the murine skin.

Heterotopic transplantation of keloid fibroblasts murine model

Preparing keloid-derived fibroblasts from passages 1–3, at a quantity of 1 × 10^7 cells then mixed with an equal volume of Matrigel, with the total volume adjusted to 200 μL per mouse. BALB/c female nude mice, that aged 6–8 weeks were anesthetized via intraperitoneal injection of sodium pentobarbital. The prepared mixture was injected into the dorsal region of the nude mice using a 1 mL syringe. Once the nodule volume reached approximately 100 mm^3, treatment was initiated. A total of 15 nude mice were randomly divided into three groups as follows: (1) Control group, receiving daily intra-tumoral injections of saline; (2) Positive control group, receiving weekly intra-tumoral injections of triamcinolone acetonide (TA) (4 mg/mL); (3) Lapatinib group, receiving daily intra-tumoral injections of lapatinib (20 μM). Treatments were administered at a volume of 50 μL per 100 mm^3 of nodule volume, with daily measurements of the dorsal nodule volume throughout the treatment period. After one week of treatment, the mice were sacrificed by cervical dislocation, and the dorsal nodules were excised for further analysis, including photography, histological examination, and assessment of gene expression levels.

CCK-8 assay

The Cell Counting Kit-8 (CCK-8) assay was utilized to evaluate the impact of the drug on fibroblast proliferation. Fibroblasts in good growth condition were plated at a density of 90% confluence, with approximately 1,000 primary cells per well in a 96-well plate. A total of 100 μL of cell suspension was aliquoted into each well and incubated in a constant temperature incubator for 24 h. Lapatinib drug solutions at the required concentrations were prepared. The culture medium in the 96-well plate was aspirated, and then 100 μL of medium containing lapatinib and 10 ng/mL TGF-β1 was added to the wells for drug treatment for one day. Each experimental group included three replicate wells to minimize error. Following a 24-hour period, 10 μL of Cell Counting Kit-8 (CCK-8) reagent was introduced to each well within a light-protected environment, and the samples were subjected to a further 4-hour incubation phase. Subsequently, the optical density of the samples was quantified at a wavelength of 450 nm utilizing a microplate spectrophotometer.

Fibroblasts migration from keloid tissue assay

Fresh keloid tissue, from which the epidermis and adipose tissue have been removed, is sectioned into 3 × 3 × 3 mm tissue cubes using a sterile surgical blade. The dermis is then placed in contact with the base of a

culture dish. Once the tissue has adhered to the dish, 10% FBS-supplemented DMEM complete growth medium is gently added to submerge the tissue cubes, taking care not to displace the tissue. Observations are made daily under a microscope, and once fibroblasts begin to migrate out of the tissue blocks, the medium is replaced with drug-containing medium supplemented with varying concentrations of lapatinib. Images are taken from the moment fibroblasts start to migrate, focusing on the same area over the course of three days, and the number of fibroblasts is quantified.

Wound healing assay

Cells are seeded in a 24-well plate, and when the cell density reaches an appropriate level, a vertical scratch is made in each well. After making the scratch, the culture medium is removed, and PBS is gently added along the scratch line. For primary mouse skin fibroblasts, 100 μL of lapatinib drug solution (concentrations of 0, 2.5, 5, 10, and 20 μM) and/or 10 ng/mL TGF-β1 is added to each well. For keloid-derived fibroblasts, lapatinib solution (concentrations of 0, 2.5, 5, 10, and 20 μM) is added to treat the fibroblasts. Cell migration is photographed at the scratch site at 0, 12, 24, 36, and 48 h using a microscope. For each time point, three different locations are selected for photography, and care is taken to ensure that the positions are consistent across different time points. Subsequently, Image J software is utilized for data analysis.

Western blot

Tissue and cellular specimens underwent lysis via a mechanical homogenization process. Protein extraction was achieved by incubating the samples for 30 min in RIPA buffer, sourced from Beyotime Biotechnology, which was supplemented with a protease and phosphatase inhibitor cocktail, prior to centrifugation at 12,000 rpm for 30 min at a temperature of 4 °C. The supernatants obtained were quantified using a BCA Protein Assay Kit. Following this, immunoblotting analysis was performed in accordance with standard protocols. Proteins were denatured by heating in loading buffer at 100 °C for 3 min before undergoing electrophoretic separation via SDS-PAGE. The resolved proteins were then transferred onto PVDF membranes, which were blocked in Tris-buffered saline with Tween-20 (TBST) supplemented with 5% non-fat milk for 1 h at room temperature. Subsequently, the membranes were incubated with primary antibodies overnight at 4 °C, followed by a 1-hour incubation with horseradish peroxidase-conjugated secondary antibodies at ambient temperature. The immunoreactive bands were visualized using a Gel Imaging System provided by Beijing Sage Creation, and the relative levels of protein expression were quantified through densitometric analysis with ImageJ software. Full-length and unaltered blots are available for review in the supplementary materials.

RT-qPCR

Trizol reagent (Beyotime) was employed for RNA isolation from clinical samples. Yeasen fluorescent real-time quantitative PCR kit was utilized. Primers, SYBR Green Mix, RNase-free water, and cDNA samples were placed in an ice box to thaw in advance. The reaction mixture was prepared according to the required experimental system and aliquoted into individual wells of an eight-tube strip, with each group having three replicates. Subsequently, cDNA was added, and the mixture was briefly centrifuged to ensure enrichment of the reaction mixture. Following the manufacturer's instructions for the qRT-PCR apparatus, amplification was performed. The data and resulting graphs obtained were used to quantitatively analyze the expression levels of the markers in the samples. This method allows for the precise measurement of gene expression and can be adapted for various applications in molecular biology and biomedical research. Target gene amplification and quantification were conducted on a Real-Time PCR Detection System (Roche) utilizing the One-Step RT-qPCR Probe Kit (Yeasen, China). Relative fold changes in gene expression were determined by normalization to housekeeping genes, GAPDH or β-Actin, employing the comparative cycle threshold (Ct) method, also known as the 2-△△Ct method. A comprehensive list of the primers used is detailed in Table 1.

Cell transfection

In this experiment, we designed two double strained siRNA against the coding sequence of ErbB1 and ErbB2, respectively (Table 2) and the TransIT-X2 transfection reagent was utilized, following the manufacturer's provided protocol. Keloid-derived fibroblasts were plated in a six-well plate and cultured for 12 h or until they achieved 80% confluence. After the transfection complex was prepared, 250 μL of the mixture was added dropwise to various areas of the six-well plate containing serum-free DMEM. The plate was gently rocked to ensure even distribution of the complex. The cells were then incubated for 24 to 48 h to facilitate transfection. Upon completion of the incubation period, the cells were harvested to extract RNA or protein. These cellular components were subsequently employed in downstream applications, including real-time qPCR assays to evaluate gene expression levels and immunoblotting techniques for the analysis of protein expression and post-translational modifications.

HYP content measurement

An equal amount (10 mg) of skin from the affected area of the mouse was weighed and placed into the ampoules, which were then dried in an oven at 120 °C for 18 h. After opening the ampoule caps, 2 mL of 6 M NaOH was added to each, and the mixture was filtered using a syringe and microporous membrane into a 10 mL centrifuge tube. The pH was then adjusted to 7.0–8.0, and the total volume was adjusted to 10 mL with ddH_2O. To each tube, chloramine T was added, vortexed to ensure thorough mixing, and then left at room temperature for 20 min. Subsequently, perchloric acid was added to each tube, vortexed, and left at room temperature for 5 min. Finally, P-DMAB was added to each tube, vortexed, and incubated in a 50 °C water bath for 20 min. After the solutions had cooled, 200 μL from each tube was aliquoted into a 96-well plate, with 3 replicates for each sample.

Gene	Primer	Sequence (5'-3')
M-GAPDH	Forward	TGGATTTGGACGCATTGGTC
	Reverse	TTTGCACTGGTACGTGTTGAT
M-α-SMA	Forward	GCTGGTGATGATGCTCCCA
	Reverse	GCCCATTCCAACCATTACTCC
M-Col1α1	Forward	CCAAGAAGACATCCCTGAAGTCA
	Reverse	TGCACGTCATCGCACACA
M-Fn	Forward	AAGGATGGAGTGATAGCAACCC
	Reverse	TCTGCTTGAAATCTGGTGTGC
H-β-actin	Forward	AGGCCAACCGTGAAAAGATG
	Reverse	AGAGCATAGCCCTCGTAGATGG
H-α-SMA	Forward	TGGGTGAACTCCATCGCTGTA
	Reverse	GTCGAATGCAACAAGGAAGCC
H-Col1α1	Forward	AAGCCGGAGGACAACCTTTTA
	Reverse	GCGAAGAGAATGACCAGATCC
H-Col3α1	Forward	TGGTGTTGGAGCCGCTGCCA
	Reverse	CTCAGCACTAGAATCTGTCC
H-Fn	Forward	GCCACTGGAGGTCTTTACCACA
	Reverse	CCTCGGTGTTGTAAGGTGGA
H-ErbB1	Forward	GGAGAACTGCCAGAAACTGAC C
	Reverse	GCCTGCAGCACACTGGTTG
H-ErbB2	Forward	AGCCGCGAGCACCCAAGT
	Reverse	TTGGTGGGCAGGTAGGTGAGTT
H-ErbB3	Forward	GTCTGTGTGACCCACTGCAACT
	Reverse	GGGTGGCAGGAGAAGCATT
H-ErbB4	Forward	GGCTGCTGAGTTTTCAAGGATG
	Reverse	GCTTCATACGATCATCACCCTGA

Table 1. Real-time PCR primer synthesis list.

siRNA	Primer	Sequence (5′–3′)
ErbB1-1	sense	CUCUGGAGGAAAAGAAAGU
	antisense	ACUUUCUUUUCCUCCAGAG
ErbB1-2	sense	CACAGUGGAGCGAAUUCCU
	antisense	AGGAAUUCGCUCCACUGUG
ErbB2-1	sense	CCUGUUCUCCGAUGUGUAA
	antisense	UUACACAUCGGAGAACAGG
ErbB2-1	sense	GGUGUGAGAAGUGCAGCAA
	antisense	UUGCUGCACUUCUCACACC
CTL		UAAUUGCAAGUGGUAGAUGTT

Table 2. SiRNA against ErbB1 and ErbB2.

The absorbance was measured at 577 nm, and the hydroxyproline content of the tissues was calculated based on a standard curve of hydroxyproline.

Histology

The skin tissues from mice were subjected to perfusion with a 4% solution of paraformaldehyde (PFA) at ambient temperature, followed by overnight immersion in PFA post-tracheal ligation. The tissues were subsequently processed by embedding in paraffin and sectioned into serial slices of 5-micrometer thickness. Histological assessment was conducted using hematoxylin and eosin (H&E) staining to evaluate tissue morphology, as well as Masson's trichrome staining to highlight collagen deposition. Furthermore, immunohistochemical staining for collagen type I (Col1), fibronectin (Fn), and alpha-smooth muscle actin (α-SMA) was performed to ascertain the extent of fibrosis within the tissue. The stained sections were examined utilizing light microscopy at a magnification of ×20, providing a detailed visualization of the fibrotic changes within the skin tissues.

Statistical analysis

Statistical analysis of the data was performed employing GraphPad Prism version 8.0 software. To evaluate the disparities among the control, model, and experimental groups, pairwise comparisons were conducted using t-tests, while one-way analysis of variance (ANOVA) was applied for assessing multiple group comparisons. All experiments were conducted independently three times to ensure the reliability and reproducibility of the results. The data are expressed as the Mean ± Standard Deviation (Mean ± SD), and statistical significance was set at a threshold of $P < 0.05$.For the quantification of Western blot band intensities, immunofluorescence signal intensities, and immunohistochemical positive signal intensities, the ImageJ software was employed. The thickness of the mouse skin epidermis was measured using the Image-Pro Plus software.

Results

Lapatinib suppresses the high expression of ErbB1 and ErbB2 in keloids

We initially investigated the expression of the ErbB family in normal skin tissue and keloid tissue, as well as in normal dermal fibroblasts and keloid fibroblasts, with quantitative reverse transcription polymerase chain reaction (qRT-PCR). The results revealed that, at the transcriptional level, ErbB1 and ErbB2 expression was increased in keloid tissues and fibroblasts, whereas ErbB3 and ErbB4 expression was decreased in these same compartments (Fig. 1A, B. This differential gene expression pattern suggests a potential role for ErbB1 and ErbB2 in the pathogenesis of keloids, possibly through the modulation of fibroblast activity and extracellular matrix production. Further studies were designed to elucidate the mechanistic contributions of ErbB1 and ErbB2 to keloid formation and progression.

The elevated expression of ErbB1 and ErbB2 in keloid tissue and fibroblasts prompted an investigation into the impact of their respective and combined gene knockouts on the activation of keloid fibroblasts and the expression of fibrotic factors. We designed two double-stranded siRNAs against the coding sequences of ErbB1 and ErbB2 (Table 2), and keloid fibroblasts were transfected with those siRNAs. The mRNA expression levels of ErbB1 and ErbB2 in keloid fibroblasts were determined by RT-qPCR, and the results revealed that ErbB1-1 and ErbB2-1 were more effective at inhibiting the expression of ErbB1 and ErbB2 (Fig. 2A). On the basis of these results, we selected ErbB1-1 and ErbB2-1 as siRNAs for subsequent experiments and found that, at the genetic level, the knockout of ErbB1 and ErbB2 in keloid fibroblasts, either individually or in combination, resulted in a decrease in the expression levels of the quintessential markers of fibroblast activation, Type I collagen (CoL-1) and fibronectin (Fn), with the combined knockout resulting in a more pronounced effect (Fig. 2B and D).

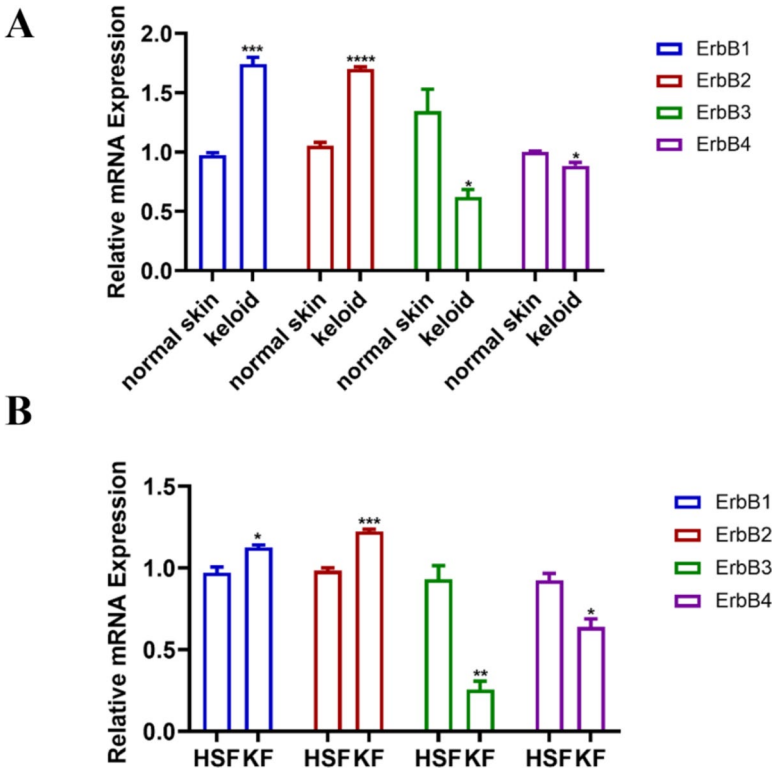

Fig. 1. ErbB1, ErbB2 are highly express in tissues and fibroblasts from keloid samples. (**A**) Relative mRNA expression of ErbB1, ErbB2, ErbB3, and ErbB4 in normal skin tissues and keloid-derived skin tissues analyzed by RT-qPCR. (**B**) Relative mRNA expression of ErbB1, ErbB2, ErbB3, and ErbB4 in Human Skin Fibroblasts (HSF) and Keloid-derived Skin Fibroblasts (KF) analyzed by RT-qPCR. The data which presented in this study are expressed as mean ± SD ($n = 3$). the statistical analysis revealed significant differences when compared with the control group, *P < 0.05, **P < 0.01, ***P < 0.001, ****P < 0.0001.

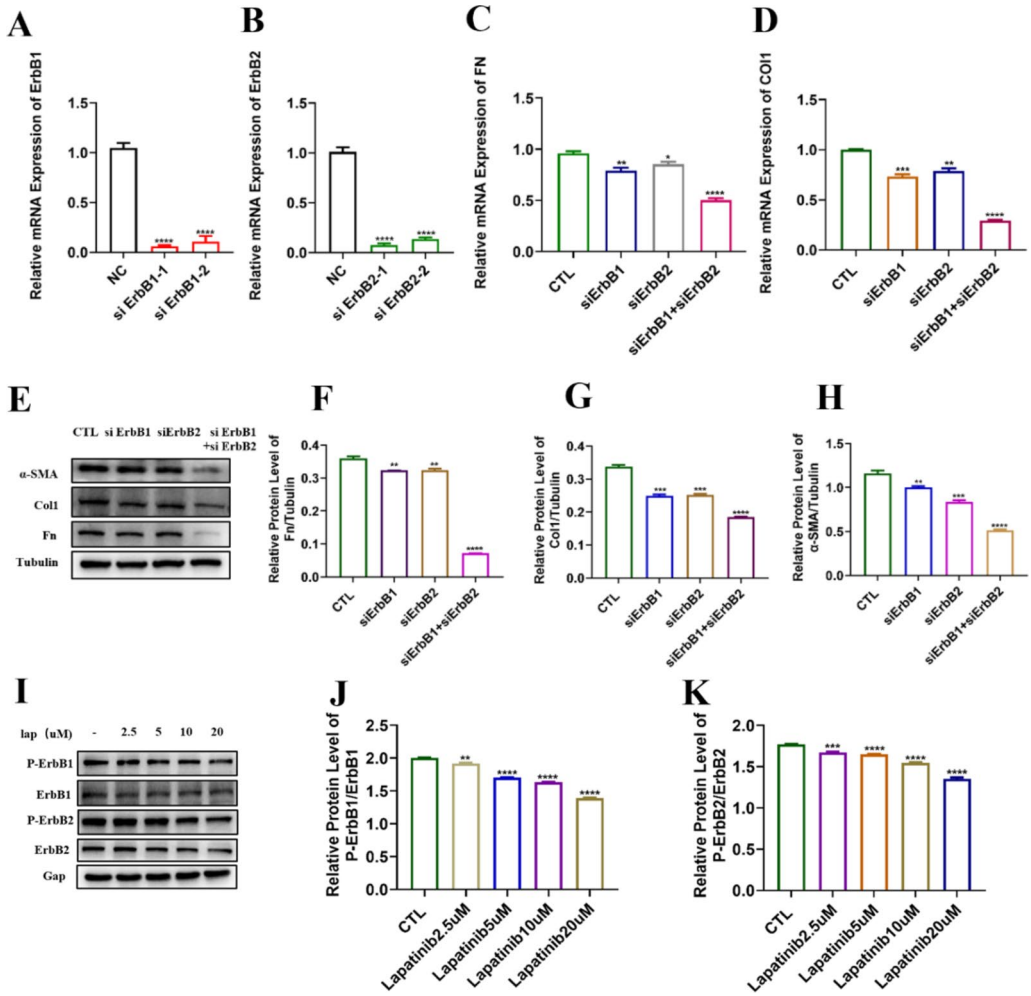

Fig. 2. Gene Knockout of ErbB1 and ErbB2 in keloid Fibroblasts Inhibits Cell Activation & Lapatinib Suppresses the Expression of ErbB1 and ErbB2 in Keloid fibroblasts. (**A**-**B**) Relative mRNA expression of ErbB1 / ErbB2 after transfection with siErbB1-1/siErbB1-2 or siErbB2-1/ siErbB2-1 in KF, analyzed by RT-qPCR. (**C**-**D**) Relative mRNA expression of fibronectin and collagen I in siErbB1, siErbB2, and siErbB1 + siErbB2 groups in KF analyzed by RT-qPCR. (**E**-**H**) The expression protein levels of fibroblast markers α-SMA, CoL-1, and Fn were assessed by Western blot analysis (**I**-**K**) The expression protein levels of phosphorylated ErbB1, phosphorylated ErbB2, ErbB1, and ErbB2 after treated with lapatinib of different concentrations in KF. The data which presented in this study are expressed as mean ± SD ($n = 3$). the statistical analysis revealed significant differences when compared with the control group, *P < 0.05, **P < 0.01, ***P < 0.001, ****P < 0.0001.

Concurrently, the protein expression levels of the fibroblast markers α-SMA, CoL-1, and Fn were assessed by Western blot analysis (Fig. 2E) and subjected to quantitative analysis (Fig. 2F and H). The findings revealed that the knockout of ErbB1 and ErbB2 in keloid fibroblasts, whether singularly or in tandem, inhibited the activation of keloid fibroblasts by reducing the expression of α-SMA, CoL-1, and Fn at both the mRNA and protein levels, with the combined knockout again showing superior efficacy.

Because the expression of ErbB1 and ErbB2 was increased in keloid tissue and fibroblasts and because of their potential influence on promoting the process of skin fibrosis[18–20], we explored the efficacy of lapatinib in treating skin fibrosis. On the basis of these findings, we conducted a pharmacological study on the efficacy of lapatinib in keloid fibroblasts. In accordance with previous studies[21–23], we selected four concentrations of lapatinib, 2.5, 5, 10, and 20 μM, for subsequent pharmacological experiments. We initially used Western blot analysis to assess the protein expression levels of the markers ErbB1 and ErbB2 and their phosphorylated proteins. As shown in Fig. 2I and K, treatment with lapatinib resulted in a dose-dependent decrease in the expression of phosphorylated ErbB1 and phosphorylated ErbB2 proteins, whereas the protein levels of ErbB1 and ErbB2 remained unchanged, which is consistent with previous studies.

According to the results mentioned above, lapatinib was used in subsequent experiments to evaluate the specific roles of ErbB1 and ErbB2 in skin fibrosis.

Lapatinib inhibits the proliferation, migration, and activation of keloid fibroblasts

The effect of lapatinib on the proliferation of keloid fibroblasts was evaluated through the CCK-8 assay. The findings revealed that, relative to the control group, the groups exposed to varying concentrations of lapatinib (2.5, 5, 10, and 20 μM) exhibited dose-dependent inhibition of cell proliferation (Fig. 3A). Additionally, the influence of lapatinib on the migratory behaviour of keloid fibroblasts was investigated with both a scratch

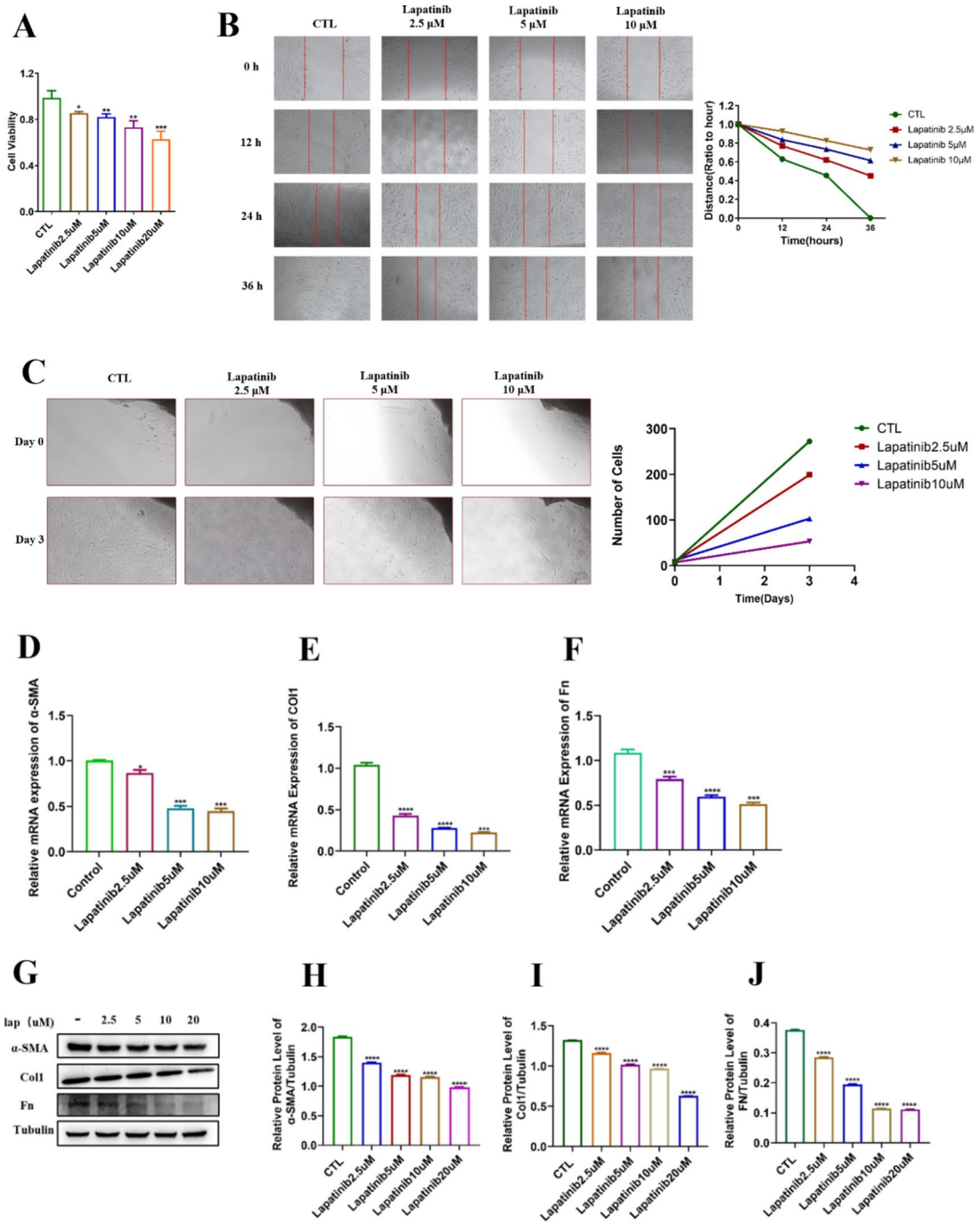

Fig. 3. Lapatinib Inhibits the Proliferation, Migration, and Activation of Keloid Fibroblasts. (**A**) CCK-8 assay of KF after treating with different concentration of Lapatinib (2.5, 5, 10, and 20 μM). (**B**) Wound-healing assay to test the effects of Lapatinib on the migration of keloid fibroblasts. (**C**) Ex vivo keloid explant culture model to examined the effects of Lapatinib's effect on inhibiting the migration of keloid fibroblast. (**D**-**F**) Relative mRNA expression of α-SMA, COL1, and FN in KF analyzed by RT-qPCR after treating with different concentration of Lapatinib (2.5, 5, 10, and 20 μM). (**G**-**J**) Relative protein expression of α-SMA, COL1, and FN in KF analyzed by Western Blot after treating with different concentration of Lapatinib (2.5, 5, 10, and 20 μM). The data which presented in this study are expressed as mean ± SD (n = 3). the statistical analysis revealed significant differences when compared with the control group, *P < 0.05, **P < 0.01, ***P < 0.001, ****P < 0.0001.

wound-healing assay and an ex vivo model involving keloid explant cultures. As shown in Fig. 3B, lapatinib significantly suppressed the migration of keloid fibroblasts at various time points (0 h, 12 h, 24 h, and 36 h) compared with that in the control group. In the keloid explant culture model, different concentrations of lapatinib were added at the onset of fibroblast migration from the edge of the keloid (Day 0). On the third day after the addition of lapatinib, images were taken under the same field of view, and the number of migrated cells was counted, which revealed that lapatinib significantly inhibited the migration of keloid fibroblasts in a dose-dependent manner (Fig. 3C).

Lapatinib suppresses the proliferation, migration, and activation of primary mouse dermal fibroblasts (PSFs) induced by TGF-β1

TGF-β1 is an important participant throughout the wound healing process, and several lines of preclinical evidence suggest that excessive production of TGF-β1 may promote the development of skin fibrosis[24–26]. To further validate whether lapatinib inhibits the development of skin fibrosis, we designed an experiment to determine the ability of lapatinib to suppress the proliferation, migration and activation of PSFs induced by TGF-β1, as observed in keloid fibroblasts.

A CCK-8 assay was used to evaluate the impact of lapatinib at concentrations of 2.5, 5, 10, and 20 μM on the proliferation of PSFs stimulated with TGF-β1. The findings revealed that TGF-β1 stimulation led to increased cell proliferation, which was markedly attenuated by lapatinib treatment in a concentration-dependent manner (Fig. 4A). A scratch wound-healing assay was subsequently utilized to investigate the influence of lapatinib on PSF migration. The experimental data indicated that lapatinib significantly impeded the migratory capacity of TGF-β1-induced PSFs compared with that of control cells. The number of migrating cells was markedly increased upon TGF-β1 induction, and this migration was notably reduced following treatment with lapatinib (Fig. 4B).

We subsequently exposed PSFs to TGF-β1 and a range of lapatinib concentrations to develop an in vitro cellular model for examining the influence of the drug on the expression of fibrotic factors. At the molecular level, treatment with lapatinib led to a dose-dependent decrease in the expression of α-SMA, a quintessential marker of fibroblast activation, relative to that in the cell group treated with only TGF-β1 (Fig. 4C). In parallel, Western blotting was utilized to assess and quantify the levels of fibroblast-specific biomarkers, namely, the α-SMA, CoL-1, and Fn proteins. These findings indicated that while the induction of TGF-β1 increased the levels of these protein biomarkers, their expression was attenuated upon lapatinib treatment (Fig. 4D, G). In summary, these experiments demonstrate that lapatinib can inhibit the proliferation, migration, and activation of PSFs induced by TGF-β1.

Lapatinib inhibits fibroblast activation in skin fibrosis via TGF-β1/Smad2/3 and non-Smad signaling pathways

Skin fibrosis is characterized by excessive deposition of dysfunctional extracellular matrix (ECM), which impedes the complete regeneration of tissue structure and function during the wound healing process. The TGF-β signalling pathway has been identified as a key player in these phenomena, indicating that interventions targeting the TGF-β pathway could enhance the outcomes of wound healing and scarring[10,27,28]. Tomasso et al.[29] demonstrated that sustained high levels of ERK activity are a hallmark of complex tissue regeneration, with the fibroblast growth factor and ErbB signalling pathways acting as upstream regulators of ERK in the regenerative process. On the basis of these studies, we hypothesize that lapatinib may inhibit fibroblast activation in skin fibrosis through both the TGF-β1/Smad and non-Smad signalling pathways. To test this hypothesis, we conducted in vitro validations with WB assays on keloid fibroblasts and PSFs.

The results indicated that treatment with lapatinib significantly reduced the protein expression levels of phosphorylated Smad2/3 in keloid fibroblasts, whereas the total protein expression levels of Smad2/3 remained unchanged. Furthermore, lapatinib also significantly decreased the protein expression levels of p-ERK and p-AKT (Fig. 5A, E). Similar experimental outcomes were validated in PSFs induced by TGF-β1 (Fig. 5F, J), suggesting a critical role of lapatinib in alleviating fibroblast activation in skin fibrosis.

Lapatinib Inhibits the proliferation and activation of xenografted keloid fibroblasts via the TGF-β1/smad and non-Smad signalling pathways

We established a xenograft model of keloid fibroblasts to assess the effects of lapatinib in a humanized animal model. Each mouse was implanted with a keloid fibroblast cluster obtained from a keloid patient, and when the cluster volume reached approximately 100 mm^2, the treatment was administered via intratumoral injection, with daily treatments for one week, after which the grafted tissues were excised for further analysis.

Initially, we measured the volume of the nodules after one week of treatment with triamcinolone acetonide (TA) as the positive control drug group, as it is commonly used in the clinical treatment of skin fibrosis[30–32], and the results revealed that the nodule volume in the lapatinib-treated group was smaller than that in the control group but that lapatinib was less effective compared with the positive control drug group (Fig. 6A). Images of the excised tissues also supported this conclusion (Fig. 6B), indicating that lapatinib inhibits the proliferation of xenografted keloid fibroblasts in nude mice.

We subsequently extracted RNA from the grafted tissues for gene expression analysis. After one week of lapatinib treatment, the expression of the fibrosis-related proteins α-SMA, Col1, Col3, and Fn in the keloid graft tissues was significantly decreased (Fig. 6C, F). Western blot experiments to assess the expression of fibrotic activation proteins in the tissues also revealed that lapatinib reduced the levels of α-SMA, Col1, and Fn in the keloid graft tissues (Fig. 6G, J). Collectively, these results suggest that lapatinib can inhibit the activation of xenograft keloid fibroblasts.

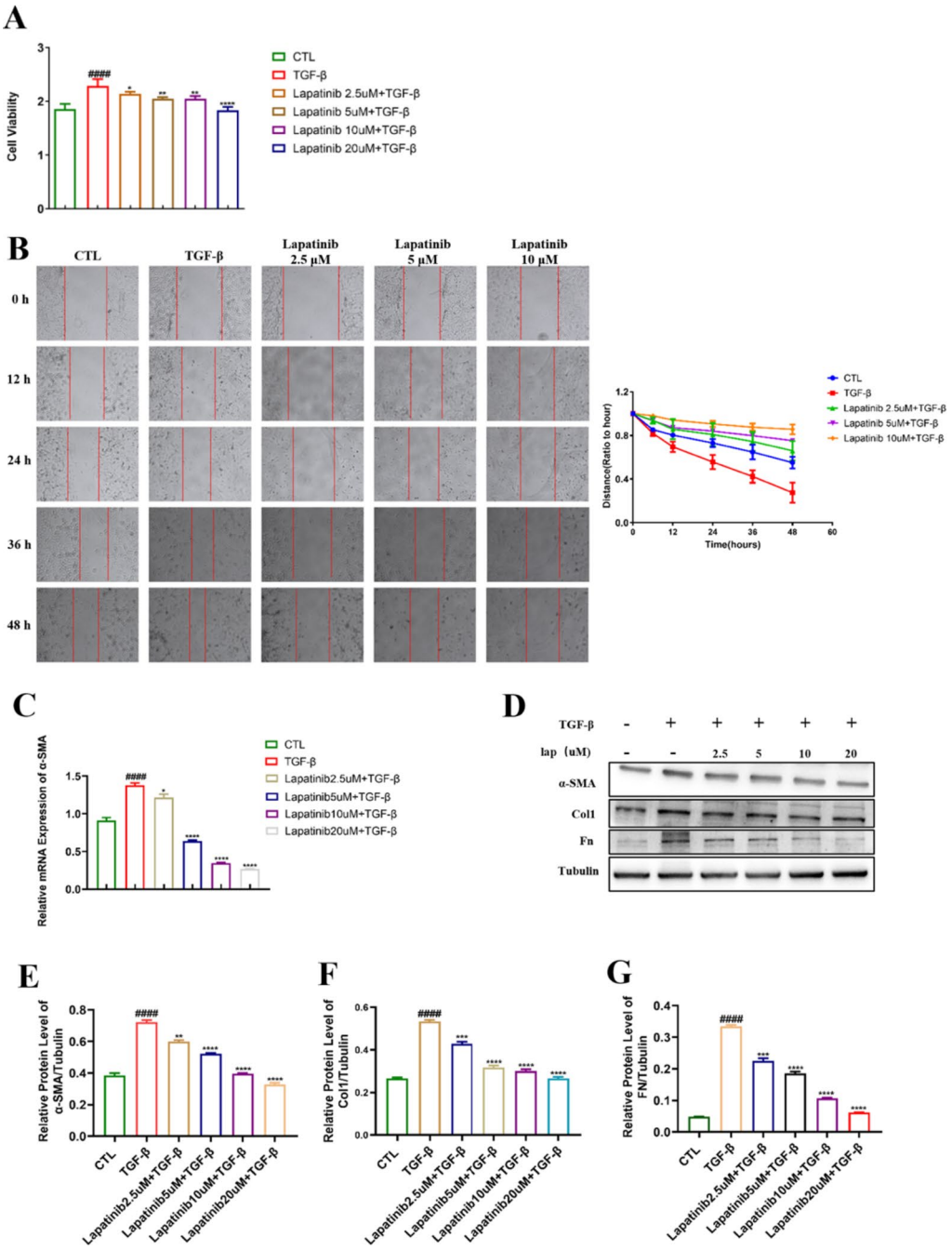

Fig. 4. Lapatinib Suppresses the Proliferation, Migration, and Activation of Primary Mouse Dermal Fibroblasts (PSF) Induced by TGF-β1 (**A**) CCK-8 assay of PSF after treating with different concentration of Lapatinib (2.5, 5, 10, and 20 μM) or/and TGF-β（10ng/ml）. (**B**) Wound-healing assay to test the effects of Lapatinib on the migration of PSF. (**C**) Relative mRNA expression of α-SMA in PSF analyzed by RT-qPCR after treating with different concentration of Lapatinib (2.5, 5, 10, and 20 μM) or/and TGF-β（10ng/ml）. (**D**-**G**) Relative protein expression of α-SMA, COL1, and FN in PSF analyzed by Western Blot after treating with different concentration of Lapatinib (2.5, 5, 10, and 20 μM) or/and TGF-β（10ng/ml）. The data which presented in this study are expressed as mean ± SD (n = 3). Statistical analysis revealed significant differences when compared with the control group, denoted as ####P < 0.0001, *P < 0.05, **P < 0.01, ***P <0.001, ****P <0.0001 as compared with TGF-β model group.

To further explore the mechanism of action of lapatinib in this model, we used Western blot experiments to examine the proteins involved in the TGF-β1/Smad and non-Smad signalling pathways in xenograft keloid fibroblasts. The results indicated that treatment with lapatinib significantly reduced the phosphorylation levels of Smad2 and Smad3 without significantly affecting the total protein levels of Smad2/3. Moreover, lapatinib markedly inhibited the protein expression levels of p-ERK and p-AKT (Fig. 6K, O).

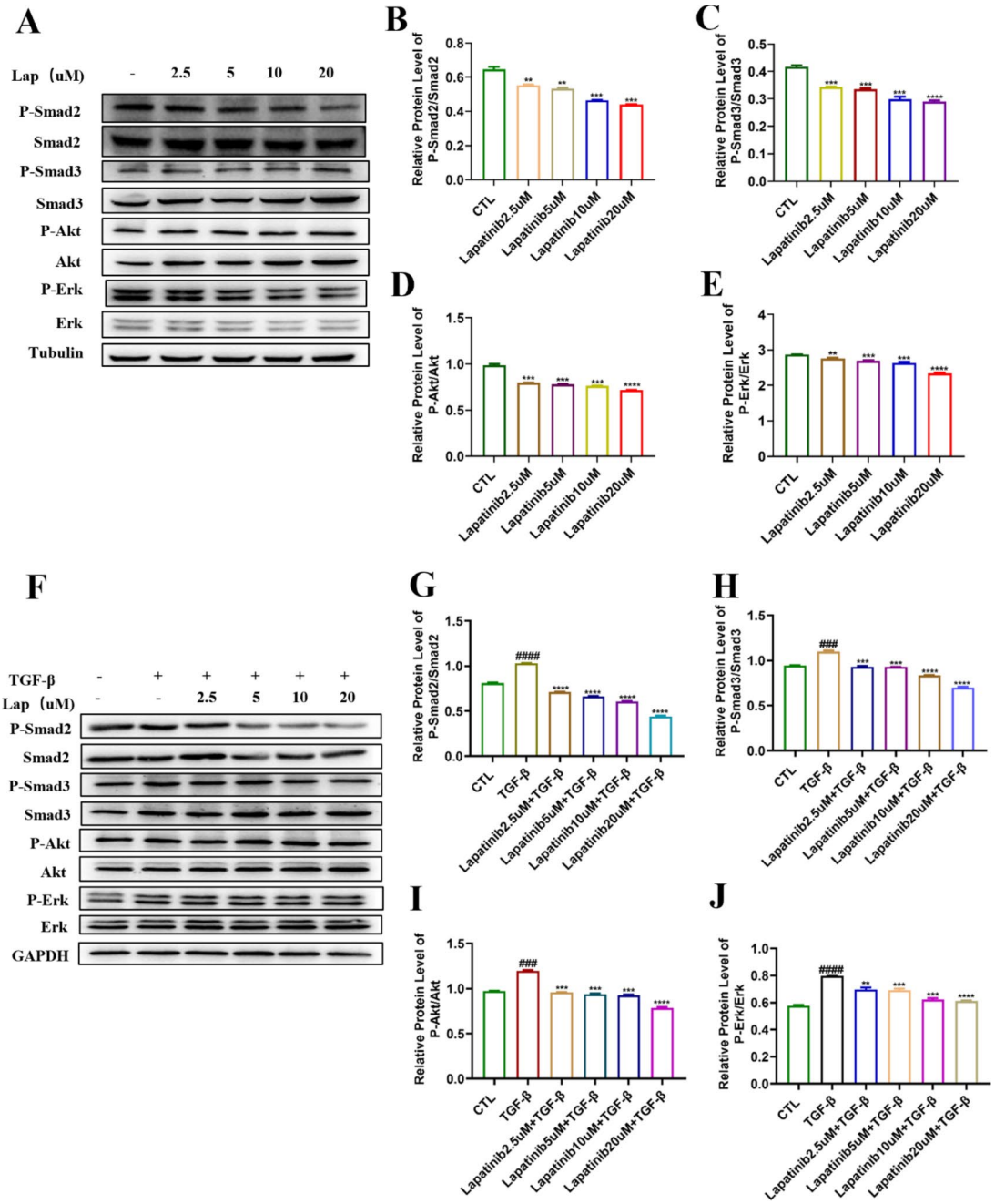

Fig. 5. Lapatinib Inhibits Fibroblast Activation in Skin Fibrosis via TGF-β1/Smad2/3 and Non-Smad Signaling Pathways (**A**-**E**) Relative protein expression of P-smad2, Smad2, Smad3, P-Smad3, Akt, P-Akt, Erk, and P-Erk in KF analyzed by Western Blot after treating with different concentration of Lapatinib (2.5, 5, 10, and 20 μM) ）. (**F**-**J**) Relative protein expression of P-smad2, Smad2, Smad3, P-Smad3, Akt, P-Akt, Erk, and P-Erk in PSF analyzed by Western Blot after treating with different concentration of Lapatinib (2.5, 5, 10, and 20 μM) or/ and TGF-β（10ng/ml）. The data which presented in this study are expressed as mean ± SD (n = 3). Statistical analysis revealed significant differences when compared with the control group, denoted as #P < 0.05, ##P < 0.01, ####P < 0.0001, *P < 0.05, **P < 0.01, ***P <0.001, ****P <0.0001 as compared with model group.

In summary, these results demonstrate that lapatinib effectively inhibits the activation of xenograft keloid fibroblasts and the deposition of collagen in a humanized animal model by TGF-β1/Smad and non-Smad signalling pathways.

Lapatinib mitigates skin fibrosis by inhibiting TGF-β1/smad and non-Smad signalling pathways to suppress fibroblast activation in a bleomycin-induced murine model

To explore the therapeutic efficacy of lapatinib on cutaneous fibrosis in vivo, we established a murine model of systemic sclerosis by administering bleomycin (0.5 U) and subsequently conducted histopathological

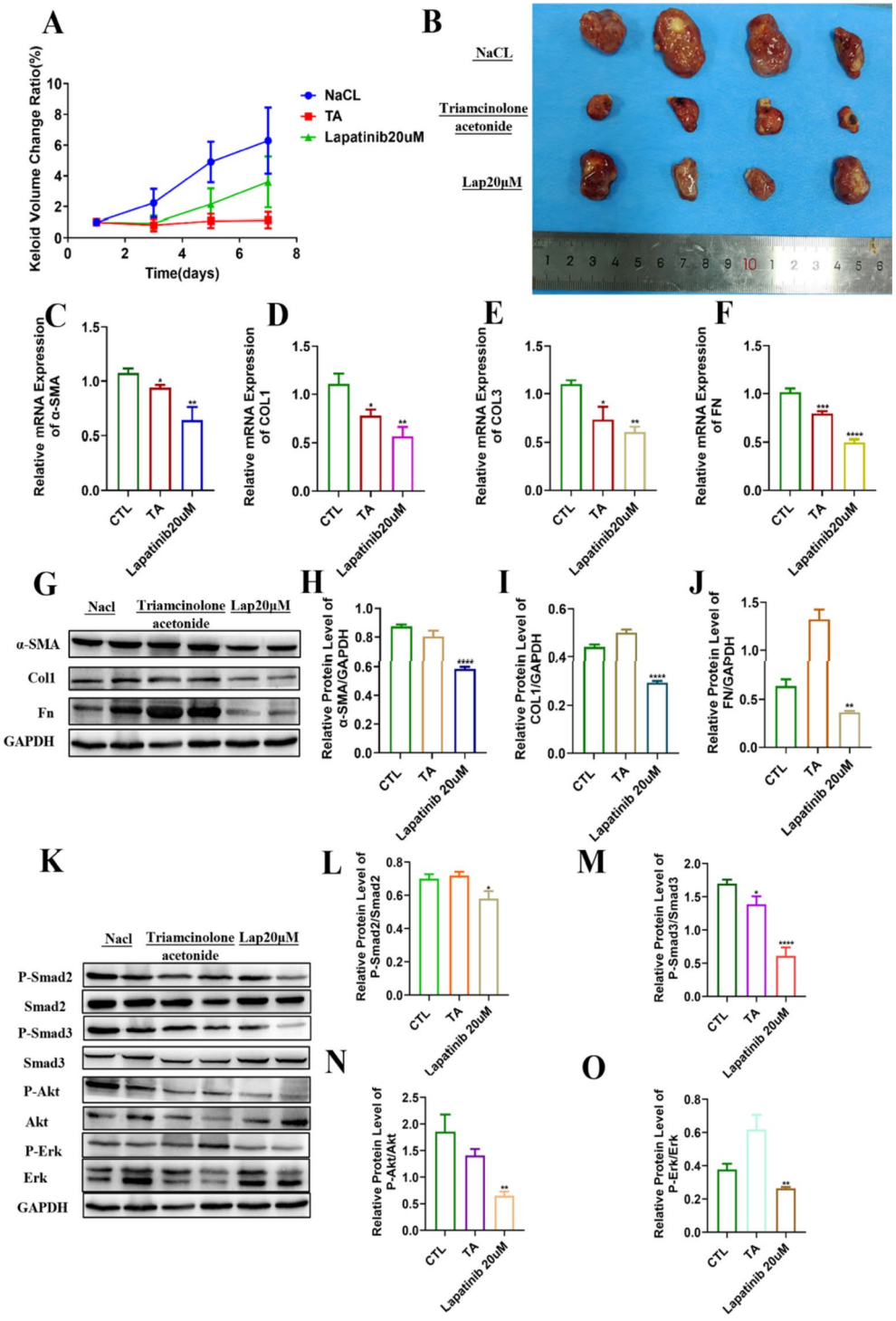

Fig. 6. Lapatinib Inhibits the Proliferation and Activation of Xenografted Keloid Fibroblasts via TGF-β1/Smad and Non-Smad Signaling Pathways. (**A**) The nodule volume in the patient-derived keloid fibroblast transplant murine model (**B**) Image of the excised tissues in each group. (**C**-**F**) Relative mRNA expression of α-SMA, COL1, COL3, and FN in the patient-derived keloid fibroblast transplant murine model analyzed by RT-qPCR. (**G**-**J**). Relative protein expression of α-SMA, COL1, and FN analyzed by Western Blot. (**K**-**O**) Relative protein expression of P-smad2, Smad2, Smad3, P-Smad3, Akt, P-Akt, Erk, and P-Erk analyzed by Western Blo The data which presented in this study are expressed as mean ± SD (n = 4). Statistical analysis revealed significant differences when compared with the control group, denoted as *P < 0.05, **P < 0.01, ***P <0.001, ****P <0.0001.

assessments of the dorsal skin[33–35]. The skin sections were subjected to haematoxylin and eosin (H&E) and Masson's trichrome staining (Fig. 7A) to evaluate the fibrotic state and quantify the dermal layer thickness. The staining results revealed that the dermal layer in the mice was considerably thicker after BLM induction, characterized by the presence of dense collagen fibres, compared to that in the NaCl group. In contrast to the model group, lapatinib treatment led to a significant reduction in BLM-induced skin fibrosis, as evidenced by a decrease in skin thickness and collagen accumulation in the mice (Fig. 7B). Furthermore, statistical analysis of dermal layer thickness confirmed that lapatinib was capable of significantly mitigating BLM-induced skin fibrosis in a murine model. Hydroxyproline content analysis of equal masses of skin revealed that the content was significantly elevated after BLM induction and was significantly reduced in a dose-dependent manner following treatment with lapatinib (Fig. 7C). Additionally, the results of the immunohistochemical staining revealed that lapatinib dose-dependently reduced the levels of α-SMA, CoL1, and Fn in mouse skin tissue (Fig. 7D, G).

The results from both the histopathological sections and the collagen content suggest that lapatinib can significantly inhibit the progression of BLM-induced skin fibrosis in a murine model.

To elucidate the in vivo efficacy and underlying mechanisms of lapatinib, protein extracts were obtained from murine skin tissues. Western blot analysis revealed that lapatinib treatment significantly downregulated the expression of the fibrotic marker proteins α-SMA and Fn in the skin tissues of mice with BLM-induced skin fibrosis (Fig. 8A,C), which aligned with the results of the immunohistochemical staining experiments. These results suggest that lapatinib can mitigate the activation of dermal fibroblasts in mice, thus ameliorating BLM-induced skin fibrosis. Additionally, we assessed the influence of lapatinib on the activation status of pivotal proteins within the TGF-β1/Smad and non-Smad signalling cascades in mice. Western blotting demonstrated that after BLM induction, lapatinib substantially reduced the phosphorylation of Smad2 and Smad3 in a dose-dependent manner without significantly impacting the total protein levels of Smad2/3. In parallel, lapatinib also significantly suppressed the protein expression levels of phosphorylated ERK (p-ERK) and phosphorylated AKT (p-AKT) (Fig. 8D, H). In conclusion, these results indicate that lapatinib mitigates skin fibrosis by inhibiting the TGF-β1/Smad and non-Smad signalling pathways to suppress fibroblast activation in a bleomycin-induced murine model.

Discussion

Skin fibrosis represents an overactive wound healing process and is a fundamental component of the aetiology of various dermatological conditions[36]. The socioeconomic impact of skin fibrosis is considerable, yet the development of efficacious and long-lasting scar management strategies continues to be a critical deficiency in clinical practice. The demand for groundbreaking therapeutic approaches that address both the prevention and treatment of dermal fibrosis and aberrant scarring is substantial and unmet[37]. Advancing our comprehension of the regulatory mechanisms underlying cytokine function and identifying novel animal models that closely mirror the human dermal fibrosis phenotype are essential steps towards the development of novel therapeutics[38]. Such advancements have the potential to not only decelerate disease progression but also to exert transformative effects on the chronicity and trajectory of these fibrotic conditions[39].

In this study, we mainly talked about the effect of lapatinib in the two types of skin fibrosis diseases. Keloids are localized, exaggerated fibrotic responses to dermal injury, while systemic sclerosis is a broader autoimmune disease affecting multiple organ systems, with skin sclerosis being one of its key manifestations. For distinctively determined the effect of lapatinib in alleviating skin fibrosis of both types of diseases, we designed both in vitro and in vivo experiment for them separately.

Fibroblasts serve as the principal effector cells under scrutiny, given their pivotal and dynamic role in sophisticated tissue repair mechanisms and the fibrotic response[40]. Recognized as the quintessential cellular agents in the pathogenesis of scarring and fibrosis, fibroblasts have become a focal point in research endeavors aimed at enhancing the outcomes of wound healing and dermal fibrosis[41]. On the basis of the empirical data supporting the importance of fibroblasts, we designed keloid patient-derived fibroblasts for keloid cell experiments and used an in vitro experiment on TGF-β-induced PSFs to mimic the pathogenesis of SSc on the basis of previous studies[42–44].

For the in vivo experiments, we established a keloid patient-derived fibroblast transplantation murine model was used. Keloids are characterized by excessive and disorganized collagen deposition within the dermis, often extending beyond the original wound margins. Our histopathological analysis in the keloid patient-derived fibroblast transplantation murine model revealed that keloid tissues exhibited a more nodular and disorganized collagen pattern and higher density of inflammatory cells. And the results showed that lapatinib could inhibit the exaggerated fibrosis primarily confined to the dermis and the tendency to form a tumor-like protrusions (Fig. 6A and B). And the results of qPT-PCR and western blot both revealed that lapatinib can inhibit the ECM deposition. As for SSc, a BLM-induced SSc murine model to determine the effect of lapatinib in SSc-lead skin fibrosis which marked by dense, hyalinized collagen fibers with a more uniform arrangement, leading to diffuse skin thickening. we conducted histopathological analyses using H&E staining and Masson's trichrome staining, and the results showed that lapatinib can significantly decreasing the dermis thickness and collagen accumulation in skin tissues (Fig. 7A C). Furthermore, the results of the immunohistochemical staining (Fig. 7D and G) and western blot (Fig. 8A C) all revealed that lapatinib dose-dependently reduced the levels of the representative biomarkers about skin fibrosis, α-SMA, CoL1, and Fn in mouse skin tissue. The expression of ErbB1 has been found to be positively correlated with organ fibrosis. Zhou et al. demonstrated that the inhibition of ErbB1 ameliorates TGF-β-induced pulmonary fibrosis[45], Savage et al. reported that ErbB1 signalling is upregulated during hepatic fibrogenesis[46], and Zhu et al. reported elevated ErbB1 expression at both the protein and mRNA levels in renal tubulointerstitial fibrosis[47]. Although ErbB1 has not been reported to be related to skin fibrosis, some studies have shown that it may be involved in some skin disorders, such as squamous cell carcinoma of the skin, cutaneous melanoma, and basal cell carcinoma of the skin[48,49]. ErbB2 has been shown to be related

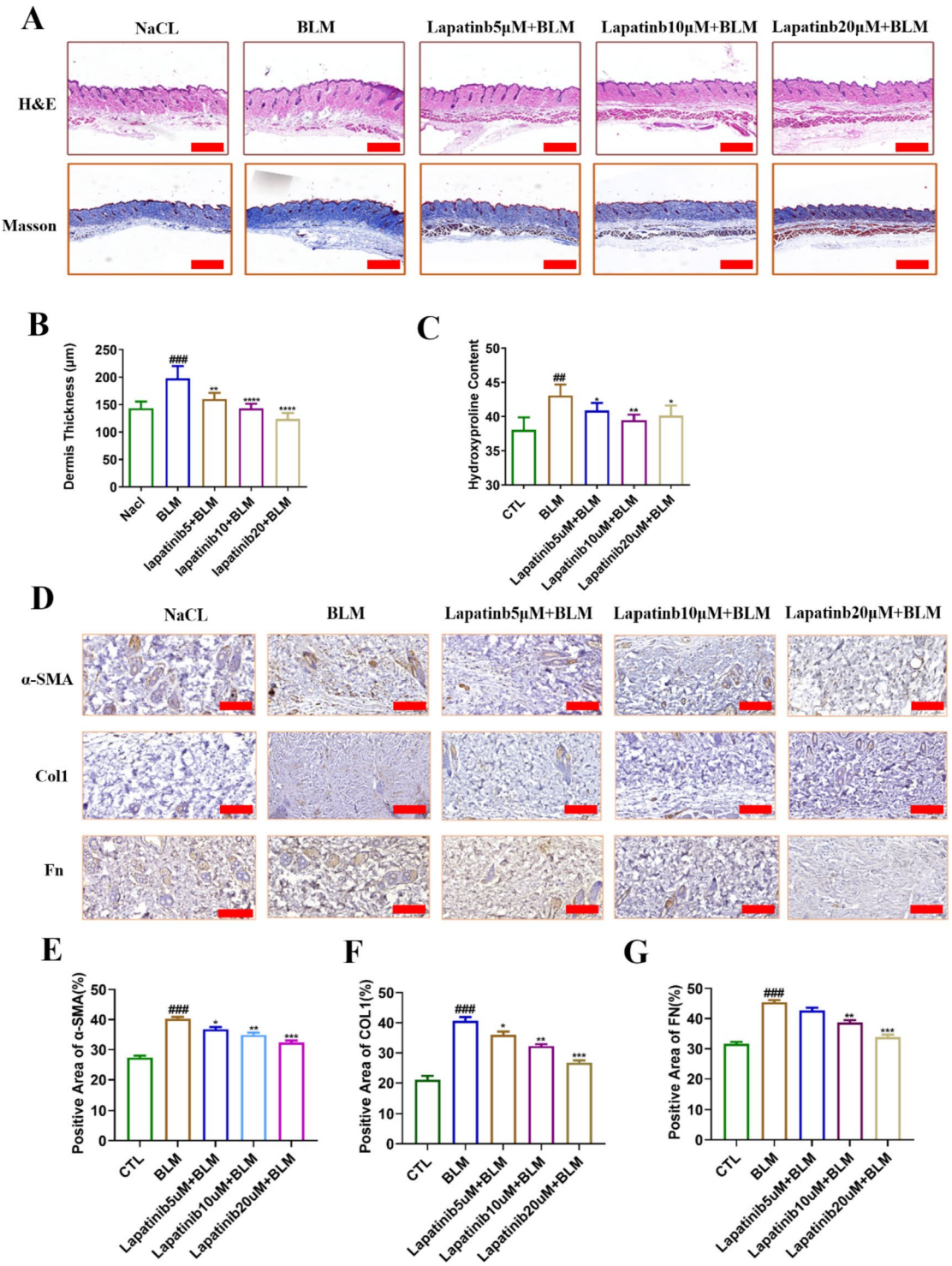

Fig. 7. Lapatinib Mitigates BLM-Induced Skin Fibrosis in Mice (**A**) H&E and Masson staining of skin tissues (Scale: 500 μm). (**B**) Quantification of skin thickness (**C**) Hydroxyproline contents in 10g skin tissues per mouse. (**D**) Immunohistochemistry was used to analyze the expression levels of α-SMA, Col1 and Fn. Quantitative analysis was shown (**E**-**G**) Scale bars: 20 μm. The data which presented in this study are expressed as mean ± SD (n = 7). Statistical analysis revealed significant differences when compared with the control group, denoted as #P < 0.05, ##P < 0.01, ####P < 0.0001, *P < 0.05, **P < 0.01, ***P <0.001, ****P <0.0001 as compared with model group.

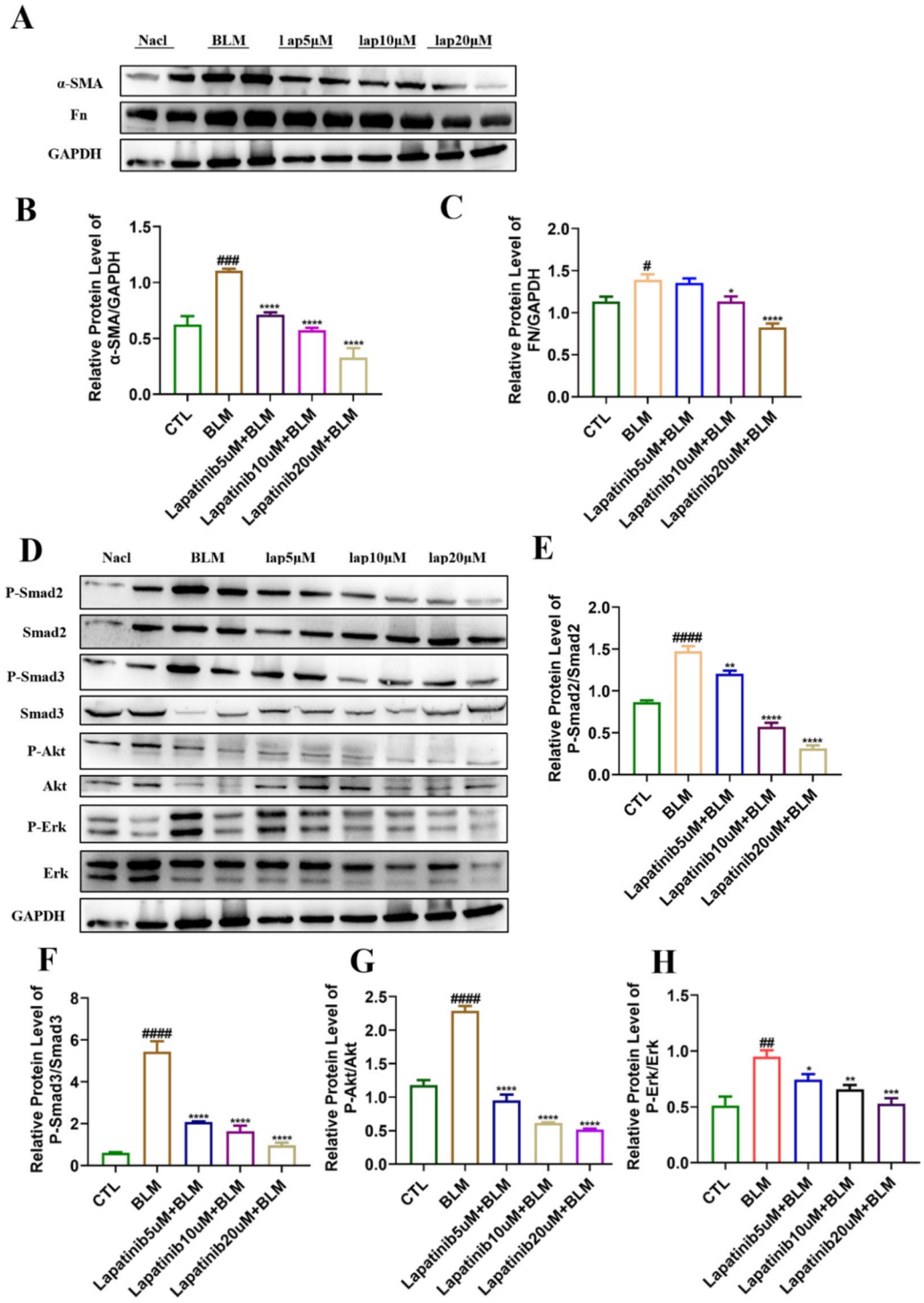

Fig. 8. Lapatinib Mitigates Skin Fibrosis by Inhibiting TGF-β1/Smad and Non-Smad Signaling Pathways to Suppress Fibroblast Activation in Bleomycin-Induced Murine Model (**A**-**C**) Relative protein expression of α-SMA and FN in BLM-induced murine model analyzed by Western Blot (**D**-**H**) Relative protein expression of P-smad2, Smad2, Smad3, P-Smad3, Akt, P-Akt, Erk, and P-Erk in BLM-induced murine model analyzed by Western Blot. The data which presented in this study are expressed as mean ± SD (n = 7). Statistical analysis revealed significant differences when compared with the control group, denoted as #P < 0.05, ##P < 0.01, ####P < 0.0001, *P < 0.05, **P < 0.01, ***P <0.001, ****P <0.0001 as compared with model group.

to organ fibrosis and to promote keloid fibrosis by Jumper, Natalie et al.[50]. Both markers, ErbB1 and ErbB2, are commonly reported in organ fibrosis but rarely in skin fibrosis. In this study, we found that these genes were highly expressed in keloid tissues and fibroblasts. To address the role of ErbB1 and ErbB2, we knocked them out by transient transfection in keloid fibroblasts and surprisingly found that the expression levels of the quintessential markers of fibroblast activation, CoL-1 and Fn, were decreased. The question thus arises as to whether an inhibitor of both ErbB1 and ErbB2 could be effective in treating skin fibrosis.

Lapatinib has been previously shown to have effects on several breast cancer cell lines[51] and patients with breast cancer[19], and its effects on skin fibrosis were evaluated. According to previous studies, lapatinib has been identified as a potential treatment for several skin disorders. Gholizadeh, Nasim et al. reported that lapatinib can block the epithelial–mesenchymal transition in nonmelanoma skin cancers by interfering with the PI3K/AKT/mTOR and Wnt/ErK/PI3K-AKT signalling pathways[52]. Yao, Ming et al. reported that lapatinib interrupted the PI3K/AKT/mTOR signalling pathway in human cSCC cells[17], and Hidaka, Takanori et al. successfully treated HER-2-positive metastatic apocrine carcinoma of the skin with lapatinib[53]. Our in vitro and in vivo results support that lapatinib can significantly alleviate skin fibrosis through the TGF-β1/Smad2/3 and non-Smad signalling pathways.

We have conducted an in-depth analysis of the pivotal role of the TGF-β pathway in skin fibrosis, with a particular focus on the involvement of ErbB1 and ErbB2 in the activation of fibroblasts induced by TGF-β, which serves as a key instigator of tissue fibrosis, exacerbating pathological reparative processes by promoting the proliferation of fibroblasts and the deposition of the extracellular matrix (ECM)[54]. Our findings reveal that TGF-β activates ErbB1 and ErbB2 in skin fibrosis, a process essential for the maintenance of the activated state of fibroblasts. Lapatinib significantly inhibited TGF-β-induced fibroblast activation in this study. This finding is congruent with the mechanism of action of lapatinib in the treatment of pancreatic cancer[55,56]; however, its potential application in the treatment of skin fibrosis was explored for the first time in this study. Although we did not stratify the various subpopulations of fibroblasts in this research, on the basis of the existing data analysis, the response is likely dependent on the ErbB1/ErbB2 signalling pathway in mesenchymal fibroblasts[57]. These findings suggest that lapatinib may selectively target the pathological fibrotic process without disrupting normal tissue repair mechanisms. Given the inhibitory effects of lapatinib on the TGF-β/ErbB1/ErbB2 signalling cascade demonstrated in this study, we propose that lapatinib may emerge as a novel therapeutic option for the treatment of skin fibrosis.

Future clinical studies are warranted to further investigate the treatment duration and potential combination with other therapeutic modalities of lapatinib. Additionally, we advocate for the development of novel fibroblast-specific genetically engineered mouse models (GEMMs) to better understand the role of ErbB1/ErbB2-activated fibroblasts in skin fibrosis in further research and to explore the combined application of lapatinib with other immunotherapeutic strategies for the treatment of skin fibrosis.

Conclusion

This research revealed that ErbB1 and ErbB2 were both highly expressed in skin fibrosis tissue and fibroblasts, which represents a pioneering evaluation of the impact of lapatinib on the aetiology of skin fibrosis through in vitro and in vivo experimental approaches. These findings revealed that the pharmacological administration of lapatinib effectively alleviated fibrotic manifestations in skin fibrosis by reducing the activation of ErbB1 and ErbB2 in fibroblasts through regulating the TGF-β1/Smad and non-Smad signalling pathways. These cellular and molecular insights have identified a critical molecular target within the fibrotic skin environment, which presents a potential therapeutic target for the treatment of skin fibrosis.

Data availability

Data is provided within the manuscript or supplementary information files.

Received: 18 December 2024; Accepted: 3 March 2025
Published online: 11 March 2025

References

1. Coentro, J. Q., Pugliese, E., Hanley, G., Raghunath, M. & Zeugolis, D. I. Current and upcoming therapies to modulate skin scarring and fibrosis. *Adv. Drug Deliv Rev.* **146**, 37–59 (2019).
2. Philippeos, C. et al. Spatial and Single-Cell transcriptional profiling identifies functionally distinct human dermal fibroblast subpopulations. *J. Invest. Dermatol.* **138** (4), 811–825 (2018).
3. El-Halwagi, A. & Agarwal, S. K. Insights into the genetic landscape of systemic sclerosis. Best practice & research. *Clin. Rheumatol.* **38** (4), 101981 (2024).
4. Hawash, A. A., Ingrasci, G., Nouri, K. & Yosipovitch, G. Pruritus in keloid scars: mechanisms and treatments. *Acta Derm Venereol.* **101** (10), adv00582 (2021).
5. Eming, S. A., Martin, P. & Tomic-Canic, M. Wound repair and regeneration: mechanisms, signaling, and translation. *Sci. Transl Med.* **6** (265), 265sr6 (2014).
6. Yarden, Y. & Pines, G. The ERBB network: at last, cancer therapy meets systems biology. *Nat. Rev. Cancer*. **12** (8), 553–563 (2012).
7. Yarden, Y. & Sliwkowski, M. X. Untangling the erbb signalling network. *Nat. Rev. Mol. Cell Biol.* **2**, 127–137 (2001).
8. Cheng, W. H. et al. Amphiregulin induces CCN2 and fibronectin expression by TGF-β through EGFR-dependent pathway in lung epithelial cells. *Respir Res.* **23** (1), 381 (2022).
9. Schramm, F., Schaefer, L. & Wygrecka, M. EGFR signaling in lung fibrosis. *Cells* **11** (6), 986 (2022).
10. Zheng, X. et al. Fibulin7 mediated pathological cardiac remodeling through EGFR binding and EGFR-Dependent FAK/AKT signaling activation. *Adv. Sci. (Weinh)*. **10** (24), e2207631 (2023).
11. VanSlyke, J. K., Boswell, B. A. & Musil, L. S. ErbBs in Lens cell fibrosis and secondary cataract. *Invest. Ophthalmol. Vis. Sci.* **64** (10), 6 (2023).

12. Wang, Q., Wang, F., Li, X., Ma, Z. & Jiang, D. Quercetin inhibits the Amphiregulin/EGFR signaling-mediated renal tubular epithelial-mesenchymal transition and renal fibrosis in obstructive nephropathy. *Phytother Res.* **37** (1), 111–123 (2023).
13. Sheng, G. et al. Reduction of fibrosis and immune suppressive cells in ErbB2-dependent tumorigenesis by an LXR agonist. PLoS One. ;16(3): e0248996.[23] McHugh, L. A. et al. Lapatinib, a dual inhibitor of ErbB-1/-2 receptors, enhances effects of combination chemotherapy in bladder cancer cells. *Int. J. Oncol.* **34**, 1155–1163 (2021).
14. Roskoski, R. Jr. The erbb/her family of protein-tyrosine kinases and cancer. *Pharmacol. Res.* **79**, 34–74 (2014).
15. Raja Sharin, R. N. F. S. et al. W. N. I. Role of ErbB1 in the underlying mechanism of lapatinib-induced diarrhoea: A review. BioMed research international, 4165808. (2022).
16. Strickley, J. D. et al. Metastatic squamous cell carcinoma of the skin with clinical response to lapatinib. *Exp. Hematol. Oncol.* **7**, 20 (2018).
17. Yao, M. et al. The research on lapatinib in autophagy, cell cycle arrest and epithelial to mesenchymal transition via Wnt/ErK/PI3K-AKT signaling pathway in human cutaneous squamous cell carcinoma. *J. Cancer*. **8** (2), 220–226 (2017).
18. Singh, D., Attri, B. K., Gill, R. K. & Bariwal, J. Review on EGFR inhibitors: critical updates. *Mini Rev. Med. Chem.* **16** (14), 1134–1166 (2016).
19. Montemurro, F., Valabrega, G. & Aglietta, M. Lapatinib: a dual inhibitor of EGFR and HER2 tyrosine kinase activity. *Expert Opin. Biol. Ther.* **7** (2), 257–268 (2007).
20. Roskoski, R. Jr Small molecule inhibitors targeting the EGFR/ErbB family of protein-tyrosine kinases in human cancers. *Pharmacol. Res.* **139**, 395–411 (2019).
21. Mona, A. M., Abo-Zeid, M. T., Abo-Elfadl, A. M. & Gamal-Eldeen evaluation of lapatinib cytotoxicity and genotoxicity on MDA-MB-231 breast cancer cell line. *Environ. Toxicol. Pharmacol. Volume* **71**,2019,103207,ISSN 1382–6689 .
22. Roos, N. J., Aliu, D., Bouitbir, J. & Krähenbühl, S. Lapatinib activates the Kelch-Like ECH-associated protein 1-Nuclear factor erythroid 2-related factor 2 pathway in HepG2 cells. *Front. Pharmacol.* **11**, 944 (2020).
23. O'Donovan, N. et al. Dual targeting of EGFR and HER-2 in breast cancer cell lines. *JCO* **24**, 13132–13132 (2006).
24. Le, M. et al. Transforming growth factor Beta 3 is required for excisional wound repair in vivo. *PLoS One*. **7**, e48040 (2012).
25. Yan, L. et al. In vitro study of TGF-β1-induced epithelial-mesenchymal transition of keloid epithelial cells. *Zhonghua Zheng Xing Wai Ke Za Zhi*. **31** (2), 128–133 (2015). Chinese.
26. Tu, Y., Lineaweaver, W. C. & Zhang, F. TGF-β1 -509 C/T polymorphism and susceptibility to keloid disease: a systematic review and meta-analysis. *Scars Burn Heal.* **3**, 2059513117709943. https://doi.org/10.1177/2059513117709943 (2017).
27. Lichtman, M. K., Otero-Vinas, M. & Falanga, V. Transforming growth factor beta (TGF-β) isoforms in wound healing and fibrosis. *Wound Repair. Regen*. **24** (2), 215–222 (2016).
28. Liu, Y. et al. TGF-β1 promotes Scar fibroblasts proliferation and transdifferentiation via up-regulating MicroRNA-21. *Sci. Rep.* **6**, 32231 (2016).
29. Tomasso, A., Koopmans, T., Lijnzaad, P., Bartscherer, K. & Seifert, A. W. An ERK-dependent molecular switch antagonizes fibrosis and promotes regeneration in spiny mice (Acomys). *Sci. Adv.* **9** (17), eadf2331 (2023).
30. Choi, Y. J., Lee, Y. H., Lee, H. J., Lee, G. Y. & Kim, W. S. Auricular keloid management in Asian skin: clinical outcome of intralesional excision and postoperative triamcinolone acetonide intralesional injection. *J. Cosmet. Dermatol.* **19** (11), 3041–3047 (2020).
31. Albalat, W., Nabil, S. & Khattab, F. Assessment of various intralesional injections in keloid: comparative analysis. *J. Dermatolog Treat*. **33** (4), 2051–2056 (2022).
32. Moravej, H., Forghanian, A., Dadkhahfar, S. & Mozafari, N. Intralesional bleomycin versus intralesional triamcinolone in the treatment of keloids and hypertrophic scars. *Dermatol. Ther.* **35** (9), e15730 (2022).
33. Cao, D. et al. ACSL4 Inhibition prevents macrophage ferroptosis and alleviates fibrosis in bleomycin-induced systemic sclerosis model. *Arthritis Res. Therapy*. **25** (1), 212 (2023).
34. Liang, Y. et al. Dynamic pathological analysis reveals a protective role against skin fibrosis for TREM2-dependent macrophages. *Theranostics* **14** (5), 2232–2245 (2024).
35. Guo, M. et al. Serum metabolomic profiling reveals potential biomarkers in systemic sclerosis. *Metab. Clin. Exp.* **144**, 155587 (2023).
36. Nguyen, J. K., Austin, E., Huang, A., Mamalis, A. & Jagdeo, J. The IL-4/IL-13 axis in skin fibrosis and scarring: mechanistic concepts and therapeutic targets. *Arch. Dermatol. Res.* **312** (2), 81–92 (2020).
37. Mokos, Z. B. et al. Current therapeutic approach to hypertrophic scars. *Front. Med.* **4**, 1–11 (2017).
38. Artlett, C. M. Animal models of systemic sclerosis: their utility and limitations. *Open. Access. Rheumatol. Res. Rev.* **6**, 65–81 (2014).
39. Beyer, C., Schett, G., Distler, O. & Distler, J. H. W. Animal models of systemic sclerosis: prospects and limitations. *Arthritis Rheum.* **62**, 2831–2844 (2010).
40. Talbott, H. E., Mascharak, S., Griffin, M., Wan, D. C. & Longaker, M. T. Wound healing, fibroblast heterogeneity, and fibrosis. *Cell. Stem Cell.* **29** (8), 1161–1180 (2022).
41. Henderson, N. C., Rieder, F. & Wynn, T. A. Fibrosis: from mechanisms to medicines. *Nature* **587**, 555–566. https://doi.org/10.1038/s41586-020-2938-9 (2020).
42. Liang, M. et al. Attenuation of fibroblast activation and fibrosis by Adropin in systemic sclerosis. *Sci. Transl. Med.* **16** (740), eadd6570 (2024).
43. Chen, Y., Gong, Y., Shi, M., Zhu, H., Tang, Y., Huang, D., Wang, W., Shi, C., Xia,X., Zhang, Y., Liu, J., Huang, J., Liu, M., Chen, H., Ma, Y., Wang, Z., Wang, L.,Tu, W., Zhao, Y., Lin, J., … Shi, X. (2024). miR-3606-3p alleviates skin fibrosis by integratively suppressing the integrin/FAK, p-AKT/p-ERK, and TGF-β signaling cascades. *J. Adv. Res.* , S2090-1232(24)00546-0. Advance online publication.
44. Mills, T. W. et al. Unraveling the role of MiR-181 in skin fibrosis pathogenesis by targeting NUDT21. *FASEB Journal: Official Publication Federation Am. Soc. Experimental Biology*, **38**(17), e70022. (2024).
45. Zhou, Y. et al. Amphiregulin, an epidermal growth factor receptor ligand, plays an essential role in the pathogenesis of transforming growth factor-β-induced pulmonary fibrosis. *J. Biol. Chem.* **287**, 41991–42000 (2012).
46. Savage, T. M. et al. Amphiregulin from regulatory T cells promotes liver fibrosis and insulin resistance in non-alcoholic steatohepatitis. *Immunity* **57** (2), 303–318e6 (2024).
47. Zhu, Q. et al. HUWE1 promotes EGFR ubiquitination and degradation to protect against renal tubulointerstitial fibrosis. *FASEB J.* **34** (3), 4591–4601 (2020).
48. Rittié, L. et al. Differential ErbB1 signaling in squamous cell versus basal cell carcinoma of the skin. *Am. J. Pathol.* **170** (6), 2089–2099 (2007).
49. Liu, S., Geng, R., Lin, E., Zhao, P. & Chen, Y. ERBB1/2/3 expression, prognosis, and immune infiltration in cutaneous melanoma. *Front. Genet.* **12**, 602160 (2021).
50. Jumper, N., Hodgkinson, T., Paus, R. & Bayat, A. A role for Neuregulin-1 in promoting keloid fibroblast migration via ErbB2-mediated signaling. *Acta dermato-venereologica*. **97** (6), 675–684 (2017).
51. Sambade, M. J. et al. Lapatinib in combination with radiation diminishes tumor regrowth in HER2 + and basal-like/EGFR + breast tumor xenografts. *Int. J. Radiat. Oncol. Biol. Phys.* **77** (2), 575–581 (2010).
52. Gholizadeh, N. et al. Revolutionizing non-melanoma skin cancer treatment: receptor tyrosine kinase inhibitors take the stage. *J. Cosmet. Dermatol.* **23** (9), 2793–2806 (2024).
53. Hidaka, T. et al. Successful treatment of HER-2-positive metastatic apocrine carcinoma of the skin with lapatinib and capecitabine. *Acta Derm Venereol.* **92** (6), 654–655 (2012).

54. Jiménez-Uribe, A. P., Gómez-Sierra, T., Aparicio-Trejo, O. E., Orozco-Ibarra, M. & Pedraza-Chaverri, J. Backstage players of fibrosis: NOX4, mTOR, HDAC, and S1P; companions of TGF-β. *Cell. Signal.* **87**, 110123 (2021).
55. Gore, J. et al. Combined targeting of TGF-β, EGFR and HER2 suppresses lymphangiogenesis and metastasis in a pancreatic cancer model. *Cancer Lett.* **379** (1), 143–153 (2016).
56. Mucciolo, G. et al. EGFR-activated myofibroblasts promote metastasis of pancreatic cancer. *Cancer Cell.* **42** (1), 101–118e11 (2024).
57. Deng, C. C. et al. Single-cell RNA-seq reveals fibroblast heterogeneity and increased mesenchymal fibroblasts in human fibrotic skin diseases. *Nat. Commun.* **12** (1), 3709 (2021).

Author contributions
Yongping Wang: Conceptualization, Data curation, Investigation, Software, Writing-original draft, Writing-review & editing; Tiantian Zhang: Conceptualization, Data curation, Investigation, Software, Writing-original draft, Writing-review & editing; Hao Song: Validation, Visualization, Writing-review & editing; Cheng Yang: Supervision, Validation, Visualization, Writing-review & editing. All authors have read and agreed to the published version of the manuscript.

Funding
This work was supported by The National Natural Science Foundation of China [Grant 82370073] and The 111 Project [Grant B20016].

Declarations

Competing interests
The authors declare no competing interests.

Ethics approval and consent to participate
All participants in our research signed an informed consent before study, and all experimental protocols done on humans were compiled by the Declaration of Helsinki and the study was approved by the Ethics Committee of Nankai University (approval No. NKUIRB2021116). All animal welfare and experimental protocols adhered to the guidelines of the Institutional Animal Care and Use Committee (IACUC) of Nankai University (Permit No. SYXK 2019-0001), and the animal study was reviewed and approved by Nankai University Animal Welfare Ethics Review Committee.All methods are reported in accordance with ARRIVE guidelines in the manuscript.

Additional information
Supplementary Information The online version contains supplementary material available at https://doi.org/10.1038/s41598-025-92687-1.

Correspondence and requests for materials should be addressed to H.S. or C.Y.